

Exergy, Energy, and Gas Flow Analysis of Hydrofractured Shale Gas Extraction

Noam Lior

Fellow ASME

Department of Mechanical Engineering
and Applied Mechanics,
University of Pennsylvania,
220 South 33rd Street,
Philadelphia, PA 19104-6315
e-mail: lior@seas.upenn.edu

The objectives of this study are to (a) evaluate the exergy and energy demand for constructing a hydrofractured shale gas well and determine its typical exergy and energy returns on investment (ExROI and EROI), and (b) compute the gas flow and intrinsic exergy analysis in the shale gas matrix and created fractures. An exergy system analysis of construction of a typical U.S. shale gas well, which includes the processes and materials exergies (embodied exergy) for drilling, casing and cementing, and hydrofracturing (“fracking”), was conducted. A gas flow and intrinsic exergy numerical simulation and analysis in a gas-containing hydrofractured shale reservoir with its formed fractures was then performed, resulting in the time- and two-dimensional (2D) space-dependent pressure, velocity, and exergy loss fields in the matrix and fractures. The key results of the system analysis show that the total exergy consumption for constructing the typical hydrofractured shale gas well is 35.8 TJ, 49% of which is used for all the drilling needed for the well and casings and further 48% are used for the hydrofracturing. The embodied exergy of all construction materials is about 9.8% of the total exergy consumption. The ExROI for the typical range of shale gas wells in the U.S. was found to be 7.3–87.8. The embodied energy of manufactured materials is significantly larger than their exergy, so the total energy consumption is about 8% higher than the exergy consumption. The intrinsic exergy analysis showed, as expected, very slow (order of 10^{-9} m/s) gas flow velocities through the matrix, and consequently very small flow exergy losses. It clearly points to the desirability of exploring fracking methods that increase the number and length of effective fractures, and they increase well productivity with a relatively small flow exergy penalty. [DOI: 10.1115/1.4032240]

Keywords: shale gas production exergy, shale gas flow and production, hydraulic fracturing, drilling for shale gas, exergy and energy return on investment

1 Introduction

The objectives of this study, started in [1], are to (a) evaluate the exergy and energy demand for constructing a hydrofractured shale gas well and determine its typical exergy and energy returns on investment (ExROI and EROI), and (b) compute the gas flow and intrinsic exergy analysis in the shale gas matrix and created fractures.

Shale gas is produced from rigid and low-permeability shale formations and is not free flowing as conventional gas. Shale formations are generally 0.6–2.1 km deep and 15–90 m thick. They are very “tight” with a general porosity around 5%, nanopores on the 10^{-9} to 10^{-6} m scale [2], and low permeability on the 10^{-3} μ D to 1μ D scale [3]. Its deep location, formation thinness, low porosity, small pores, and low permeability obviously make it harder to extract than conventional gas resource. Nevertheless, the gradual depletion of conventional gas resources and the fact that natural gas is the most desirable fossil fuel for most stationary applications because of its lowest emissions, including those of greenhouse gases, and ease of combustion, and not the least, the fact that in the U.S. it needs not be imported, shale gas accounts for most of the growth in supply from today’s recoverable gas resources.

Based on a survey of 42 countries (including the U.S.), The U.S. Energy Information Administration (EIA) estimated [4,5] the global proved technically recoverable resource (TRR) of shale gas at the end of 2013 as 97 trillion cubic feet (TCF), $= 2.75 \times 10^{12}$ m^3 , which is 1.4% of all global proved TRR gas. Adding the unproven TRR raises the total proved and unproved TRR shale

gas TRR to 7299 TCF (2.1×10^{14} m^3), while the proved and unproven nonshale natural gas TRR = 15,583 TCF, so the total proved and unproved technically recoverable gas, shale + nonshale TRR = 15,583 + 7299 = 22,882 TCF (4.4×10^{14} m^3). It is thus impressive that the relatively new global shale gas TRR constitutes 47% of the total global gas TRR increase, even more so when noting that only a small fraction of the world shale gas reservoirs were surveyed so far.

Globally, 32% of the total (proven + unproven) estimated natural gas TRR are in shale formations. The top ten countries, in order of TRR, were China, Argentina, Algeria, USA, Canada, Mexico, Australia, South Africa, Russia, and Brazil, and many other countries including Poland, UK, Germany, and India are actively exploring their resources. Global shale gas production, with the vast majority from U.S., grew at a compound annual average rate of nearly 50% from 2006 to 2010 and became 40% of the U.S. dry gas production.

The most common method for extraction of gas from shale is vertical, followed by horizontal, drilling of a well, and then hydraulic fracturing (fracking) of the gas-containing shale from it (Fig. 1, Ref. [6]). About 45,000 such wells were drilled in the U.S. (estimated from Ref. [7]). The latter process fractures the shale by high-pressure fracking liquid pumped to high pressure into the well to release the gas from its pores. Horizontal drilling extends the well laterally within the thin (mostly horizontal) shale layer to increase the contact area with the productive layer. “Wagon wheel drilling,” in which several horizontal wells are drilled from a single vertical one, minimizes the drilling work per unit product, and even more importantly, the ground surface affected.

Described in more detail, after exploration a vertical well is drilled to reach the shale layer, and then, the direction of the drilling bit is changed to horizontal [8–10] for continuing the drilling inside the shale layer to increase the contact with the reservoir.

Contributed by the Advanced Energy Systems Division of ASME for publication in the JOURNAL OF ENERGY RESOURCES TECHNOLOGY. Manuscript received November 3, 2015; final manuscript received November 10, 2015; published online February 1, 2016. Editor: Hameed Metghalchi.

For example, in the Marcellus Shale in Pennsylvania, a well that is only vertical may be exposed to as little as 15 m of the gas-bearing formation while a horizontal well may have a lateral wellbore extending in length from about 600 to 1800 m within the typically 15 to 90 m thick formation [11].

After the well is drilled, casing and cementing are applied to seal the gas production environment from the natural environment, as shown in Fig. 2 [12,13]. Usually, four layers of casing with different lengths are used to seal the well from its geological surroundings. Cement is used to fill the gaps between casings. After that, perforating “guns” are inserted to designed points to create initial fractures. Then, fracturing fluid with proppants is pumped at high pressure into the formation to generate and prop up fractures. After one stage (length) of fracturing is performed, the fractured part is sealed from the rest of the well and another stage of fracturing is performed, and this is repeated usually 15–20 times. After the fracturing process is completed, the well is cleaned and gas is allowed to flow out, first with the fracking fluid flowback and alone after the fracking fluid is thereby drained. More detailed well completion information about shale gas wells is in Refs. [14] and [15].

2 Exergy Analysis for the Shale Gas Extraction Processes

2.1 About Exergy Analysis. As described above, shale gas extraction consumes a significant amount of energy, exergy, and materials, and this study focuses on the exergy-related return on investment, ExROI, but also calculated the better known EROI, to estimate their value and provide guidance on ways for reducing the exergy destruction and energy consumption, and thus increasing the ExROI and EROI for given gas output. We performed an exergy analysis of the overall process and of all its components, including the embodied exergy. No such analysis was found in the literature.

Exergy analysis can be done on a system level or/and on an internal level [16,17], with the “system-level” analysis conducting an exergy input–output on a black box system without considering the internal process. Such an analysis can determine the exergy efficiency of each operation unit and step, including drilling, casing and cementing, and fracturing, and the exergy output of produced gas, for guidance to ways to increase the overall efficiency and the EROI. It does not, however, deliver the detailed information about the specific process phenomena, often space- and time-dependent, which causes the exergy changes in it. The phenomena may include heat transfer, mass transfer, fluid mechanics, chemical

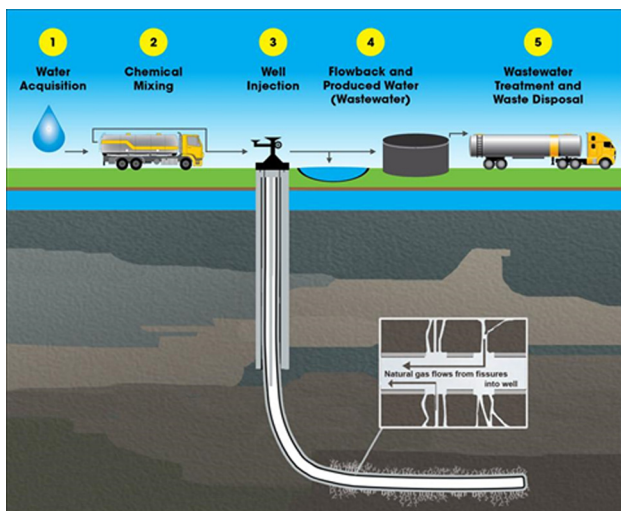


Fig. 1 Typical hydrofracturing for shale gas and the associated water cycle, from Ref. [6]

and/or nuclear reactions, and the presence of fields such as gravitational, electric, and magnetic. This type of detailed analysis, called “intrinsic” [16,17], due in the second phase of system development, is invaluable in accelerating the understanding of exergy losses and in facilitating the discovery of ways to reduce them. It requires the knowledge of the detailed multidimensional, time-dependent flow, heat and mass transfer, and mechanical processes and fields. Both system and intrinsic analyses were conducted in this study.

2.2 The System-Level Analysis. The system exergy analysis addressed the major units including drilling, casing, cementing, fracturing, and the exergy output from gas production. Processes not included are exploration, field licensing and leasing, well pad construction, and transportation of all needed materials.

2.2.1 Drilling. The most used method, horizontal drilling, mentioned above, is considered here. Since shale depth varies significantly, from being exposed on the ground to more than a thousand meters deep underground, for this analysis the depth of the currently very productive Marcellus Shale was used (which is mostly in the U.S. states of New York, Pennsylvania, Ohio, Maryland, West Virginia, Virginia, and Kentucky). For the most part, Marcellus Shale is situated in a depth of 0.6–2.1 km [18], 1.5 km was taken as the calculation depth. The horizontal part also varies according to different shale formations and treatments, typically up to 2.6 km [19], so a lateral length of 2.6 km was taken for the analysis.

Data for energy requirement for drilling shale gas wells are not readily available, so data from a comprehensive study of drilling for geothermal wells from Sandia National Laboratories [20] were used, which reported that it takes about 120 days to drill a 20,000 ft (6100 m) long well and that the fuel consumption is 2500 gal per day (9.46 m³/day). The drilling rate is reported to be approximately constant, independent of the depth. Based on the well and casing dimensions given in Ref. [20], the volume of soil drilled for this well is 1016 m³.

Assuming that the fuel used is only diesel, with density = 840 kg/m³, the fuel consumption per 1 m³ soil drilled is thus 939 (kg fuel)/(m³ drilled soil). The average specific exergy of diesel fuel is about 44 MJ/kg [21,22] (its specific energy is nearly the same), so the exergy consumption for drilling 1 m³ soil is 41 GJ/m³. We note, however, that the energy requirement is not a

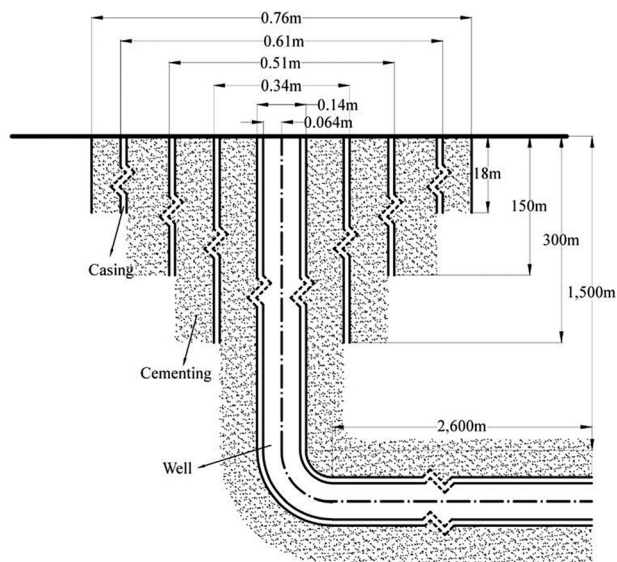


Fig. 2 Typical casing (using three casings) and cementing between the casings, dimensions specific to sources on Marcellus Shale [12,13]

linear function of volume of soil drilled, and that it depends on the ground composition. It was also assumed that the energy consumptions for drilling vertically or horizontally are the same on average. The values calculated here are therefore specific to these dimensions and conditions, which are, however, reasonably typical.

Based on the dimensions in Fig. 2, the volume of soil that is drilled for the considered shale gas well is 345 m³ and for its casings and cementing 77 m³, so the total drilled soil volume is 422 m³. The respective diesel fuel oil exergy consumptions for these drilling tasks are thus 14,145 GJ for the well and 3157 GJ for the casing and cementing, thus with the total exergy consumption for drilling $E_{\text{drill}} = 17,302$ GJ.

2.2.2 Piping, Casing, and Cementing. After drilling, several piping, casing, and cementing operations are performed to separate the gas production environment from the natural environment [23]. The casing length depends on the depth of different geological stratifications, so typical data from Refs. [8], [9], and [23] were used here. Typically, four casing and cementing operations are made, as shown in Fig. 2.

All the casings and piping are standard API pipe [24], so the volume of steel used for this casing and piping was 16.5 m³. The embodied exergy of steel at 298 K and 101,325 Pa is 374.3 kJ/mol (= 6.68 MJ/ton) [25], the density is 7874 kg/m³, and the molar mass is 0.056 kg/mol, thus 2.32×10^6 mol (129.9 ton) of steel were used, so the steel total embodied exergy is $E_{\text{steel}} = 868$ GJ.

The spaces between the casings are filled with cement, so the volume of cement used is 307 m³, and with its density of 2010 kg/m³ and exergy of 6.56 kJ/kg [26], the total embodied exergy of the used cement is $E_{\text{cement}} = 4$ GJ. The total embodied exergy consumption of casing and cementing materials is thus $E_{\text{c\&c}} = E_{\text{steel}} + E_{\text{cement}} = 872$ GJ.

This study was focused on exergy analysis but it is very noteworthy that there exists a very big difference between the embodied exergy and embodied energy values of most manufactured materials, where the energy values depend on the way they were manufactured while the exergy values usually do not. Based on world average recycled content, pipe steel embodied exergy is 24.9 MJ/kg [27], thus 3.7-fold higher than its exergy. As to cement, concrete is used in practice and its embodied energy is about 1 MJ/kg [27], thus 152-fold higher than its embodied exergy.

2.2.3 Hydrofracturing. After the casing and cementing, the casing surrounding the horizontal section of the well through the shale formation is perforated using small explosives to enable the flow of hydraulic fracturing fluids out of the well into the shale and the eventual flow of natural gas out of the shale into the well. Up to tens of perforations are created, and we thus used 25 for the calculations. It is hard to determine the exergy use for perforating and it is assumed here to be relatively negligible. After perforation, water containing a few percent chemical additives (“slickwater”) is pumped at high pressure into the well to create fractures. Since the amount of chemical additives is relatively small, the fracturing fluid was considered to be pure water.

2.2.3.1 Exergy for pumping. The exergy needed for pumping the fracturing fluid during the fracturing operation, E_{pf} , which we based on the exergy of the fuel that generates the electricity needed to drive the fracturing pump, which is also approximately of the fuel needed to drive it via a diesel engine, can be expressed as the product of the required exergetic power for that purpose, P_{ef} , multiplied by the length of time needed for the fracturing, τ_f

$$E_{\text{pf}} = P_{\text{ef}} \tau_f = \frac{P_f}{\eta_p \varepsilon_{\text{pg}}} \tau_f = \frac{Q_f (\Delta p)_f}{\eta_p \varepsilon_{\text{pg}}} \tau_f \quad (1)$$

where P_f is the required pumping power, η_p is the efficiency of the pump, here = 0.6, ε_{pg} is the power generation exergy efficiency, = 0.4, Q_f is the fracturing fluid flow rate that is typically 5–15 m³/min, here = 11.4 m³/min, $(\Delta p)_f$ is the fracturing pressure,

typically 15–100 MPa, assumed here $(\Delta p)_f = 70$ MPa, and 180 min of pumping is assumed for each stage, so assuming 25 stages (all data from Ref. [28]), here $\tau_f = 4500$ min.

The pumping power is thus $P_f = 13.3$ MW, and the total required exergy for the assumed typical fracturing job is $E_{\text{pf}} = 15,000$ GJ.

2.2.3.2 Water usage exergy. Approximately, 2000 m³ water is used for each fracturing stage, so for the assumed 25 stages, the total water usage is 50,000 m³ [28]. Its density at 298 K and 101,325 Pa is 1000 kg/m³, and its exergy at this state is 0.9 kJ/mol [25]. Thus, the embodied exergy of the used water is $E_{\text{water}} = 2500$ GJ.

2.2.3.3 Proppant usage exergy. Approximately, 210 tons of proppant is used for each fracturing stage [28], so for the assumed 15 stages, the total use of proppant is 3150 tons. Since the proppant is primarily sand, it was assumed to be pure quartz, which has an exergy = 2.2 kJ/mol [25], so the embodied exergy of proppant used is $E_{\text{proppant}} = 120$ GJ.

The total exergy required for the overall fracturing is

$$\begin{aligned} E_{\text{frac}} &= E_{\text{pf}} + E_{\text{water}} + E_{\text{proppant}} = 15,000 + 2500 + 120 \\ &= 17,620 \text{ GJ} \end{aligned} \quad (2)$$

The exergy consumption of these three main processes, drilling, casing and cementing, and fracturing, is thus

$$\begin{aligned} E_{\text{input}} &= E_{\text{drill}} + E_{\text{c\&c}} + E_{\text{frac}} = 17,302 + 872 + 17,620 \\ &= 35,794 \text{ GJ} \end{aligned} \quad (3)$$

Table 1 summarizes the exergy of each component and process and the totals.

Figures 3 and 4 show the hydrofracturing exergy use shares in making a gas well and in overall making of a hydrofractured gas well. As stated above, the embodied exergy of manufactured materials, here mostly the steel and concrete, are significantly larger than their exergy, so if the embodied energy is calculated for this case (Table 1), the total energy consumption would be 38,742 GJ, about 8% higher than the exergy. Some obvious targets for reducing the exergy and energy consumption are in more effective drilling, employment of multistage fracturing, and using less water. The latter is even more desirable for reducing water consumption and environmental damage.

2.3 Well Productivity and the ExROI. Natural shale gas production varies significantly among wells at different sites of different basins. According to Ref. [29], which summarized 107 well productions in Barnett Shale, well productions range from 0.3 Bcf (8.5×10^6 m³) per 5 yrs to 3.6 Bcf (100×10^6 m³) over 5 yrs, which is a somewhat typical life of shale gas wells.

The components of produced gas also vary among different shale basins. According to Ref. [30], 50% of the gas in the wells of the Barnett, Marcellus, Fayetteville, New Albany, and Haynesville shales contain at least 90% methane, and 93% of them contain more than 80% methane, so it was assumed here to be 90%. This study did not take into account the exergy needed for the separation of the natural gas from commercially undesired components. The exergy of pure methane is 831.6 kJ/mol [25] (nearly the same as its heating value). The ExROI is the exergy ratio of the well-life quantity of produced methane, to the above-calculated exergy investment into making a well, E_{input} . The volume of produced methane that is needed to compensate for E_{input} , V_{methane} , is thus

$$\begin{aligned} V_{\text{methane}} &= \frac{E_{\text{input}}}{0.9 e_{\text{CH}_4}} \times M_{\text{CH}_4} = \frac{35,794 \times 10^9}{0.9 \times 831,600} \times 0.016 \\ &= \frac{635,111}{0.656} \\ &= 1.17 \times 10^6 \text{ m}^3 = 0.041 \text{ Bcf} \end{aligned} \quad (4)$$

Table 1 Exergy input of the fracking operation units

Processes	Process components	Embodied exergy, GJ	Process exergy, GJ	Exergy totals, GJ
Drilling	For well		14,145	17,302
	For casing and cementing		3157	
Casing and cementing materials	Steel	868		872
	Cement	4		
Fracturing	For pumping		15,000	17,620
	For water	2500		
	For proppant	120		
Totals		3492	32,302	35,794

i.e., $1.17 \times 10^6 \text{ m}^3$ extracted gas will cover the total exergy input calculated above, and that based on the 0.3–3.6 Bcf range per well for the total five-year production

$$\text{ExROI} = \frac{0.3}{0.041} \text{ to } \frac{3.6}{0.041} = 7.3 \text{ to } 87.8 \text{ yrs} \quad (5)$$

This indicates that the considered lowest productive wells generate 7.3-fold the exergy investment while the most productive ones will produce 87.8-fold the exergy investment. A more exact assessment requires knowledge of the cumulative production as a function of time.

If embodied energy of the steel and concrete is used instead of their exergy, the EROI is about 8% lower than the ExROI, so $\text{EROI} = 6.7\text{--}81$, still indicating a satisfactory return for most of the operating wells [30] considered in this example.

It is noteworthy that these calculated values of the ExROI and EROI are slightly on the optimistic side because some smaller exergy and energy investments, such as well pad construction, materials transportation, perforation, fracking fluid mixing, gas purification, gas distribution, and the labor for all, were neglected in this analysis.

2.4 Intrinsic Exergy Analysis of Gas Transport in the Matrix and Hydraulic Fractures

2.4.1 Reservoir Modeling. The intrinsic analysis of exergy and its destruction and loss due to the gas flow during its generation in the reservoir during production require modeling of the process and the resulting pressure and velocity distribution. This analysis generates information about the flow and pressure in the gas-containing shale gas reservoir matrix and fractures, which is important and useful even if the exergy is not studied. While the number of published studies on shale gas reservoir modeling is accelerating, process complexities and large variety of fields and their materials properties did not yet allow rigorous understandings and generally acceptable results [31,32]. Many studies (e.g., Refs. [31] and [33–37]) reported predictions of gas production rates and achieved a good match with field results, but did not

focus on the fluid mechanics and hence did not adequately reveal the gas transport process.

After hydraulic fracturing, gas starts to flow from the high-pressure low-permeability matrix to the formed lower-pressure high-permeability hydraulic fractures. The shale gas reservoir is usually [2,37–42] assumed to be a “dual porosity” system, in which the matrix block and the fractures made in it are characterized by different (but constant) porosities and permeabilities, treated therefore as two interconnected different porous media. The gas flow through them is typically assumed in the literature to be one-dimensional. A “triple porosity” model in which the matrix is composed of two parts, one with microcracks and the other with macrocracks, with the additional region of the fractures made in it has also been proposed and solved [42]. It idealized the flow as one-dimensional radial by assuming that all the matrix blocks are spheres surrounded by cracks and fractures and discusses the effect of parameter changes on pressure, but does not show validation. Later, some authors proposed that due to the very low permeability and nanopores, the effects of Knudsen diffusion and slip flow are not negligible, and thus proposed pressure-dependent permeability. The study of Shabro et al. [43] numerically modeled the reservoir as concentric circles with one-dimensional radial gas flow and examined the contribution of different transport processes (advective flow, Knudsen diffusion, slip flow, and desorption) to quantify their corresponding contributions to the overall flow. Analytical modeling was done in Ref. [2] by assuming the reservoir as a dual porosity system with a pressure-dependent permeability due to Knudsen diffusion and slip flow. It assumed spherical matrix blocks attached to each other, with the fractures represented by surrounding gaps. It introduces a numerical algorithm to forecast gas production in organic shale, which simultaneously takes into account gas diffusion in kerogen, slip flow, Knudsen diffusion, and Langmuir desorption. It focuses on prediction of gas production rates but does not give a detailed explanation about the pressure and velocity distribution of the gas transport in the matrix and fractures.

It was pointed out in Refs. [32], [37], [44], and [45] that the stress and flow interactions between two or more hydraulic fractures and the interaction between a hydraulic fracture and a

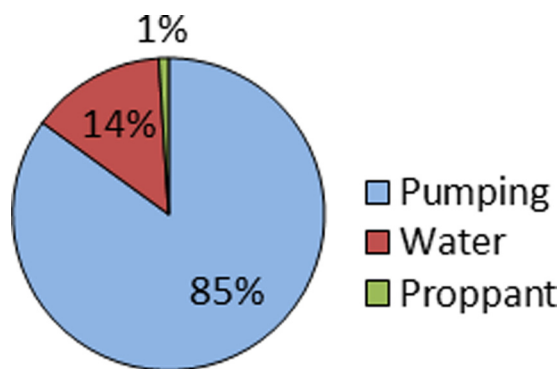


Fig. 3 Hydrofracturing exergy use shares in making a gas well

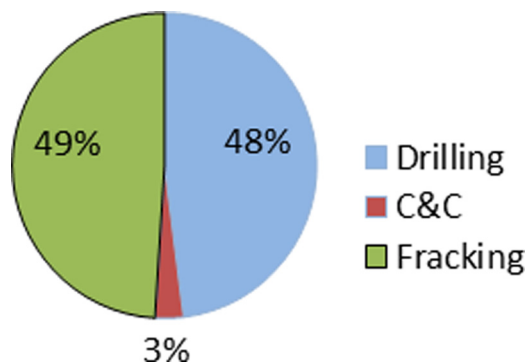


Fig. 4 Exergy use shares in overall making of a hydrofractured gas well

natural crack are important for understanding complex fracture networks and may be used in determining hydraulic fracture placements to create a complex fracture network. Further, while most studies assume for simplicity that transport coefficients are isotropic, consideration of their actual anisotropy results in better understanding and design of the desired higher flows within the matrix. When placing multiple transverse fractures in a reservoir, it is important to optimize the distance between them, because a distance that is too small can cause merging of fractures that results in low coverage of the gas drainage area, while a distance that is too large will limit the number of fractures to be created and thus reduce well productivity.

Here we propose and use an analytical model based on Refs. [2], [37], and [41] and assume that the matrix and fractures are square blocks as shown in Fig. 5, considering Knudsen diffusion and slip flow. Importantly, the gas flow in the matrix is assumed to be 2D. The gas flow in the fractures creates a variable pressure on the matrix-fracture boundaries along the fracture, thus also leading to 2D gas flow in the matrix. This is a more precise and detailed pressure and velocity distribution in the matrix and fractures, and hence, also provides a better understanding of the exergy and exergy loss change of the gas transport in matrix and fractures than obtained by the available one-dimensional ones.

Proppants, in the form of small hard particles (such as sand) that are usually added to the hydrofracturing liquid for keeping the fractures open, are likely to affect the gas flow, but their presence and flow effects were not directly considered in modeling. While rigorous analysis should include that (e.g., Ref. [46]) present models already must contend with much uncertainty about materials properties and fracture shapes in a very extensive inhomogeneous time-varying medium, and rigorous consideration of proppants would require unavailable knowledge of the particles' position and size distribution. Similar to other analyses, we, however, do incorporate it into the value of the porosity and permeability.

2.4.2 Modeling of Gas Transport From the Shale Matrix to the Hydraulic Fractures. In this model, the spacing of hydraulic fractures is assumed to be uniform and the length of all hydraulic fractures to be equal, so the matrix blocks between adjacent hydraulic fractures are also of equal dimensions. They are horizontally symmetric about the midline of the hydraulic fractures and vertically symmetric about the midline of the horizontal well, so only one matrix block is drawn in Fig. 5. The analysis control volume is half of the matrix (the cross-hatched block) and half of the hydraulic fractures adjacent to it.

The pressure gradient between the fracture and matrix causes the gas to flow from the matrix to the fractures along the

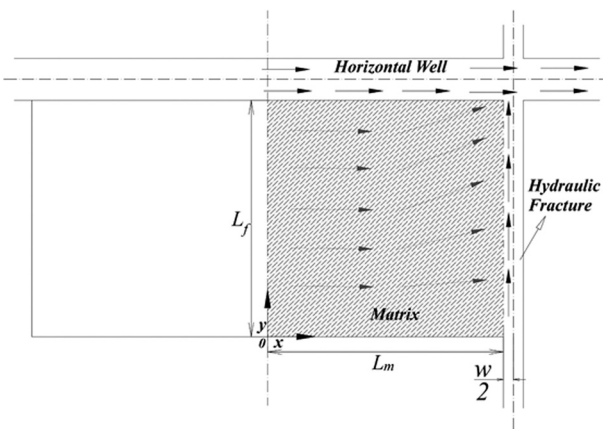


Fig. 5 Model diagram. The gas moves down the pressure gradient (left to right and up) from the undisturbed low-porosity reservoir matrix to the formed fractures, which then transport it to the horizontal well. Lines of symmetry are shown dashed and arrows show the direction of gas flows.

x -direction. The gas flow in the fracture causes a pressure gradient along the fracture, in the y -direction, and thus changes the pressure difference between the fracture and the matrix along the same direction, causing also y -directional gas flow in the matrix. L_f is the length of each hydraulic fracture. L_m is the half-width of each matrix block between two adjacent hydraulic fractures.

Model assumptions are as follows:

- Hydraulic fractures are two-wing fractures (which propagate in two “wings” being 180 deg apart and identical in shape and size) growing perpendicular to the fracking part of the well.
- Hydraulic fractures are symmetric with respect to the midline of the well.
- Hydraulic fractures are straight slim cuboids.
- Hydraulic fractures are distributed evenly along the well.
- Each hydraulic fracture looks the same (symmetric with respect to the midline between two hydraulic fractures).
- The shale matrix and the hydraulic fracture zone are treated as two porous media.
- The gas is ideal.
- The entire system (matrix and hydraulic fracture) is isothermal.
- The gas flow in the matrix is 2D, and the gas flow in the hydraulic fractures is one-dimensional (Fig. 5).

The governing equations for the gas flow from the matrix block to the hydraulic fractures are shown below.

The continuity equation in the porous shale matrix [2,37,41] is

$$\frac{\partial(\rho\phi)}{\partial t} + \nabla \cdot (\rho\mathbf{u}) = 0 \quad (6)$$

where ρ is the density, ϕ is the porosity, and \mathbf{u} is the velocity vector.

Because 2D flow velocity is assumed here, Eq. (6) becomes

$$\frac{\partial(\rho\phi_m)}{\partial t} + \frac{\partial(\rho u_x)}{\partial x} + \frac{\partial(\rho u_y)}{\partial y} = 0 \quad (7)$$

where ρ is the density of the gas, ϕ_m is the matrix porosity (assumed constant), u_x is the x -direction gas transport velocity in matrix, and u_y is the y -direction gas transport velocity in matrix. x and y are the flow direction coordinates shown in Fig. 5.

Because shale matrices have very low permeability ($10^{-3} \mu\text{D}$ to $1 \mu\text{D}$) [3] and nanopores (10^{-9} to 10^{-6} m) [2], the permeability is pressure-dependent [3]. As shown and used in the related literature (e.g., Refs. [2], [3], and [41]), Knudsen diffusion and slip flow of gas molecules play very important role in gas flow transport through nanopores and strongly enhance the flow transport in shale matrices. References [2] and [3] incorporated this influence into a modified permeability named “apparent permeability.” The apparent permeability changes with pressure and is influenced by fluid properties in addition to matrix properties, which are the only factors influencing the commonly used permeability definition. Experiments [3] showed a good agreement of an apparent permeability defined in Eq. (8) with flow behavior in such a porous material

$$k_{\text{app}} = \frac{r^2}{8} + \sqrt{\frac{8RT}{\pi M} \left[\frac{2}{3MP} + \frac{\pi}{8P} \left(\frac{2}{\alpha} - 1 \right) \right]} \mu r \quad (8)$$

where k_{app} is the apparent permeability, r is an equivalent pore-throat radius, M is the molar weight of gas molecules, P is pressure, and α is an empirical coefficient with $\alpha = 0.8$ usually used for shale rock. The average pressure was used in Ref. [3], but for better correctness, we use the actual location- and time-dependent pressure.

Replacing the common constant permeability with this modified apparent permeability, Darcy’s law using the apparent permeability is

$$u = -\frac{k_{app}}{\mu} \Delta P \quad (9)$$

Because the gas is assumed to be ideal, the density is related to pressure as

$$\rho = \frac{PM}{RT} \quad (10)$$

Expressing the velocities by Eq. (9) and using Eq. (10), Eq. (7) can be expressed as

$$\frac{\partial P}{\partial t} = \frac{1}{\mu \phi_m} \frac{\partial}{\partial x} \left(k_{app} P \frac{\partial P}{\partial x} \right) + \frac{1}{\mu \phi_m} \frac{\partial}{\partial y} \left(k_{app} P \frac{\partial P}{\partial y} \right) \quad (11)$$

To nondimensionalize, set $X = x/L_m$, $Y = y/L_f$ so using Eqs. (11) and (9), the governing equation becomes

$$\frac{\partial P}{\partial t} = \frac{1}{\mu \phi_m L_m^2} \frac{\partial}{\partial X} \left(k_{app} P \frac{\partial P}{\partial X} \right) + \frac{1}{\mu \phi_m L_f^2} \frac{\partial}{\partial Y} \left(k_{app} P \frac{\partial P}{\partial Y} \right) \quad (12)$$

that can be solved for $P(X, Y)$.

The initial pressure in the matrix is P_i . At the midline of each matrix block (at $x = 0$), the gas flow in the x -direction is symmetrically distributed about the midline. The $x = 0$ boundary is a no-flow boundary, and thus $\partial P / \partial X(0, Y, t) = 0$. At the $X = 1$ ($x = L_m$) boundary, the pressure in the matrix is assumed to be equal to the pressure in the hydraulic fractures P_f , which changes along the hydraulic fracture due to the fluid flow through it. At the $Y = 0$ ($y = 0$) boundary, assumed here that the pressure is always P_i because this is the borderline between the considered matrix and the rest of the very large shale formation which could be regarded as a pressure sink. $Y = 1$ ($y = L_f$) is the borderline between the shale matrix and the horizontal well. Because this borderline is in practice cased using steel, it permits no direct flow from the matrix to the horizontal well, so it is a no-flow boundary and $\partial P / \partial Y(X, 1, t) = 0$.

Thus, the differential equation used for gas transport within the matrix toward hydraulic fractures is Eq. (13), with boundary and initial conditions as follows:

The initial condition is

$$P(X, Y, t = 0) = P_i \quad (13)$$

and the boundary conditions are

$$\frac{\partial P}{\partial X}(0, Y, t) = 0 \quad (14)$$

$$P(1, Y, t) = P_f(Y, t) \quad (15)$$

$$P(X, 0, t) = P_i \quad (16)$$

$$\frac{\partial P}{\partial Y}(X, 1, t) = 0 \quad (17)$$

2.4.3 The Governing Equations for the Gas Flow Through any Hydraulic Fracture. Due to the proppants settling in the fractures, the hydraulic fractures are also assumed to be a porous medium, but with a much bigger constant permeability than that of the matrix.

The fracture continuity equation is

$$\frac{\partial(\rho \phi)}{\partial t} + \nabla \cdot (\rho \mathbf{u}) = F \quad (18)$$

where F is the source term representing the gas flow from the matrix.

The source term F can be calculated as in Refs. [2] and [41] by

$$F = \frac{\rho \times q}{L_m \times L_f \times w/2} \Big|_{x=L_m} = -\frac{\rho}{L_m \times L_f \times w/2} \times L_m \times L_f \times \frac{k_{app}}{\mu} \times \frac{\partial P}{\partial x} \Big|_{x=L_m} \quad (19)$$

which using Eq. (11) becomes

$$F = -\frac{M \times k_{app}}{R \times T \times \mu \times w/2} \times P \times \frac{\partial P}{\partial x} \Big|_{x=L_m} = -\frac{M \times k_{app}}{R \times T \times \mu \times w/2 \times L_m} \times P \times \frac{\partial P}{\partial X} \Big|_{X=1} \quad (20)$$

where q is the flow rate and w is the hydraulic fracture width.

Using F in Eq. (19) gives

$$\frac{\partial P_f}{\partial t} = \frac{k_f}{\mu \phi_f L_f^2} \frac{\partial}{\partial Y} \left(P_f \frac{\partial P_f}{\partial Y} \right) - \frac{k_{app}}{L_m \mu \phi_f w/2} P \frac{\partial P}{\partial X} \Big|_{X=1} \quad (21)$$

where P_f is the gas pressure in the fractures, ϕ_f is the porosity of the hydraulic fracture, and k_f is the permeability of the fracture assumed constant.

Initially, the pressure in the hydraulic fractures is the same as that in matrix, P_i . Since the fractures have much bigger permeability than the matrix, the pressure in them drops quicker than that in the matrix, this causing a pressure difference between the fractures and the matrix. At the $Y = 0$ ($y = 0$) boundary, it was assumed that the pressure is always P_i because this is the borderline between the considered fracture and the rest of the shale formation which could be regarded as a pressure source reservoir. At the $Y = 1$ ($y = L_f$) boundary, the pressure is assumed to be equal to the gas well pressure P_w , which is assumed to be constant.

The equations for gas transport through hydraulic fractures toward the horizontal wells (21) with boundary and initial conditions are as follows:

Initial condition is

$$P_f(Y, t = 0) = P_i \quad (22)$$

and the boundary conditions are

$$P_f(Y = 0, t) = P_i \quad (23)$$

$$P_f(Y = 1, t) = P_w \quad (24)$$

The data inputs for the analysis are from Ref. [43], summarized in Table 2.

2.5 Exergy Equations Derivation and Calculation. Now that the flow and pressure fields are known, the exergy and its destruction can be calculated, based on Ref. [47]. The flow specific exergy e is

$$e = h - h_0 - T_0(s - s_0) + \frac{\mathbf{V}^2}{2} + gz \quad (25)$$

where h is enthalpy, T is temperature, s is entropy, \mathbf{V} is velocity, g is gravitational acceleration, and z is altitude above a reference level. Terms with subscript 0 refer to dead state properties, which are 298 K and 101,325 Pa.

For ideal gas at constant temperature, h remains constant throughout the system, and its value for methane at the conditions indicated by the input data and at the dead state is from Ref. [48]: at the initial conditions, $P_i = 17.2$ MPa, $T = 423$ K, and $h = 226$ kJ/kg; at the well-fracture boundary condition, $P_w = 8.6$ MPa, $T = 423$ K, and $h = 259$ kJ/kg. The relatively small

Table 2 Summary of parameters used for the numerical analysis (from Ref. [43])

	Value	Units
Pore throat, r	2×10^{-9}	M
Molar mass of methane, M	1.6×10^{-2}	kg/mol
Gas dynamic viscosity, μ	1.75×10^{-5}	Pa·s
Matrix porosity, ϕ_m	0.05	N/A
Hydraulic fracture porosity, ϕ_f	0.45	N/A
Hydraulic fracture half-length, L_f	100	m
Half of the width of matrix, L_m	30.5	m
Hydraulic fracture width, w	0.3	m
Hydraulic fracture thickness, h_f	1	m
Hydraulic fracture permeability, k_f	1×10^{-10}	m ²
Initial pressure, P_i	1.72×10^7	Pa
Pressure in horizontal well, P_w	8.6×10^6	Pa
Temperature, T	423	K
Dead state temperature, T_0	298	K
Dead state pressure, P_0	101,325	Pa

change in h despite the large pressure difference follows the ideal gas assumption, and therefore, the average, 243 kJ/kg, was used as the enthalpy of gas in the considered system. The enthalpy of methane at dead state, $P_0 = 101,325$ Pa and $T_0 = 298$ K, is $h = -1.3$ kJ/kg.

The entropy change ideal gas at constant temperature is

$$s_2 - s_1 = -R \ln \frac{P_2}{P_1} \quad (26)$$

So, in Eq. (25)

$$s - s_0 = -R \ln \frac{P}{P_0} = -R \ln \frac{P(x,t)}{P_0} \quad (27)$$

Thus, the exergy in the matrix and fractures is

$$e(X, Y, t) = h - h_0 + T_0 R \ln \frac{P(X, Y, t)}{P_0} + \frac{\mathbf{V}(X, Y, t)^2}{2} + gz \quad (28)$$

Since initially flow velocity is zero, the exergy loss is thus

$$\begin{aligned} e_{\text{loss}} &= T_0(s_2 - s_1) + \frac{V_1^2 - V_2^2}{2} = T_0 R \ln \frac{P_1}{P_2} + \frac{V_1^2 - V_2^2}{2} \\ &= T_0 R \ln \frac{P_i}{P} - \frac{V^2}{2} \end{aligned} \quad (29)$$

where $P \equiv P_m$ when calculating the e_{loss} for the matrix, and $P \equiv P_{\text{hf}}$ in the hydraulic fracture.

The equation system described above, with its initial and boundary conditions, was implemented in and solved by the COMSOL MULTIPHYSICS[®] finite element analysis solver and simulation software [49]. Solution error analysis and validation are presented in Sec. 2.8.

2.6 Results and Discussion

2.6.1 The Pressure, Velocity, and Exergy Loss Distributions in the Matrix. The numerical analysis was performed for periods up to 15 days following the fracking, and the pressure, velocity, and exergy loss fields are shown in Figs. 6–9.

The gas flow from the shale matrix is primarily driven by the pressure difference between the matrix, assumed here to be initially at a pressure of 1.72×10^7 Pa, toward the lowest pressure point of the well's horizontal pipe assumed to be at 8.6×10^6 [40]. Figures 6–9 show that the gas pressure in the matrix is being reduced toward larger values of X because the fracture that drains the gas to the well is along $X = 1$ and the lowest pressure is at the

upper right corner ($X = 1, Y = 1$) where the gas flows from the fracture to the well's horizontal pipe (that is, along $Y = 1$). It is therefore also clear why the gas pressure is highest at the lower left corner ($X = 0, Y = 0$), that is, at the center of this matrix and thus furthest from the gas drainage zone. It can also be seen that the distribution changes with time from nearly symmetric about the diagonal line formed between the lower left corner and the upper right corner, to nearly vertical (i.e., along Y) at later times. The reason is that the bottom line ($Y = 0$) is the border over which gas from the rest of the formation will diffuse to the considered matrix, but the top line ($Y = 1$) is the casing that does not allow gas to pass through to the well except at ($X = 1, Y = 1$), where the fracture meets the drainage pipe.

The results show that the pressure change rate in the matrix decreases with time, as expected, and becomes nearly stable after about 5 days, after which it changes very slowly to a stable pressure distribution after about 15 days.

The velocity in the matrix corresponds to the pressure distributions and is seen to be very low, generally on the 10^{-9} m/s scale. The highest velocities are understandably around the upper right corner, at the junction between the matrix, fracture, and well. They are 1.5×10^{-9} to 3×10^{-9} m/s and increasing with the closeness to that junction. The velocities gradually decrease with time as the continuous flow reduces the driving pressure difference.

The very low velocities in the matrix indicate that the exergy loss in it would also be very low, especially relative to the extracted gas exergy, but the exergy loss distributions provide some useful information about the process. The exergy loss of the gas in the matrix changes by at most 0.5% of the total (here of 287.6 kJ/kg), because the enthalpy and gravity components of the exergy do not change and the kinetic energy term (in Eq. (29)) is negligibly small (on a 10^{-18} scale versus exergy loss on a 10^0 scale), and thus, its loss is almost entirely due to the entropy increase determined by pressure change. The exergy loss changes rapidly within the initial 5 days and changes more and more slowly until the 15th day, and then becomes stable.

While the exergy loss is very small, the reason is the low flow rate through the shale matrix for the hydrofracturing design and configuration described in this model that is typical in many current shale gas extraction systems. It clearly points to the desirability of exploring fracking methods that increase the number and length of fractures, which would increase well productivity at a relatively small exergy penalty as calculated here and in Sec. 2.

2.6.2 Pressure, Velocity, and Exergy Loss Distributions in the Hydraulic Fracture. The computations in the fractures were made from 1 to 60 s after the start; at about 60 s, the pressure and flow field in the fractures reach a steady state.

The computed pressure distribution in the hydraulic fracture is shown in Fig. 10(a), exhibiting that the pressure decreases with time and its drop gradient rises as the junction point ($Y = 1$) is approached. The pressure at any time instant decreases from the high assumed value of 17.2 MPa to the low one of 8.6 MPa. It decreases with time because, as shown above, the transport velocity within the matrix and from it to the hydraulic fracture is too low to provide gas to the fracture quickly enough to maintain the pressure in it as it conducts the gas to the horizontal well.

It is also seen that the pressure in the fractures becomes increasingly stable (linear), even after a time as short as 60 s, which is much sooner than the time for the matrix gas pressure to stabilize, due to the much higher permeability and larger pressure difference along the hydraulic fracture.

Since the gas velocity in the fracture (Fig. 10(b)) is proportional to the pressure gradient, it is seen to indeed relate to the pressure field. In the range of about $Y = 0.6-1$, it decreases with time, as the gas amount originally in the fracture is being depleted due to its flow to the well, while in the $Y = 0-0.6$ range, it increases with time due to gas transport from the matrix along the fracture. Since the initial amount of gas in the fracture is small and flows rapidly

to the well, its velocity in the $Y=0.6-1$ range declines within the first 10s, and then due to its exhaustion but the simultaneous increase of inflow from the matrix, the velocity decrease rate slows down and approaches a stable situation after about 60 s.

The exergy loss of gas in the hydraulic fracture (Fig. 10(c)) increases with time and Y , caused by the pressure drop at the corresponding time and location, and is only about 0.6% of the gas exergy (here of 271.7 kJ/kg). Just as the pressure (Fig. 10(a)), it increases faster initially, with a decreasing change rate with time, and becomes stable after about 60 s, when the gas flow from the matrix becomes sufficient to maintain a stable pressure distribution in the fracture.

It appears that the fracture width and length are adequate to drain the flow from the pores of the matrix in this model; in other words, the flow resistance in the fracture is smaller than that in the matrix pores. This should be an important criterion in designing hydrofracturing systems.

2.7 Sensitivity Analysis. As also shown in the model equations, the pressure, velocity, exergy, and exergy loss of the gas in the matrix and hydraulic fractures are affected by r , the equivalent pore-throat radius that affects the permeability of the matrix; ϕ_m , the matrix porosity, which affects the gas content in the matrix and gas transport; P_i , the initial pressure, which affects the pressure distribution; k , the permeability of hydraulic fractures, which affects the gas transport in the fractures; ϕ_f , the fracture porosity, which affects the initial gas content in the fractures and gas transport; L_f , the length of hydraulic fractures determined by the fracturing treatment, which affects the fracture pressure drop; w , the width of fractures determined by the fracturing treatment, which also affects the fracture pressure drop; and L_m , the width of the matrix, i.e., the distance between fractures. Noting that the gas transport initially changes strongly in a short time and then reaches a stable situation for a long time, our sensitivity analysis was confined to that steady state. The results of the analysis of the computed effects of these parameters are shown below.

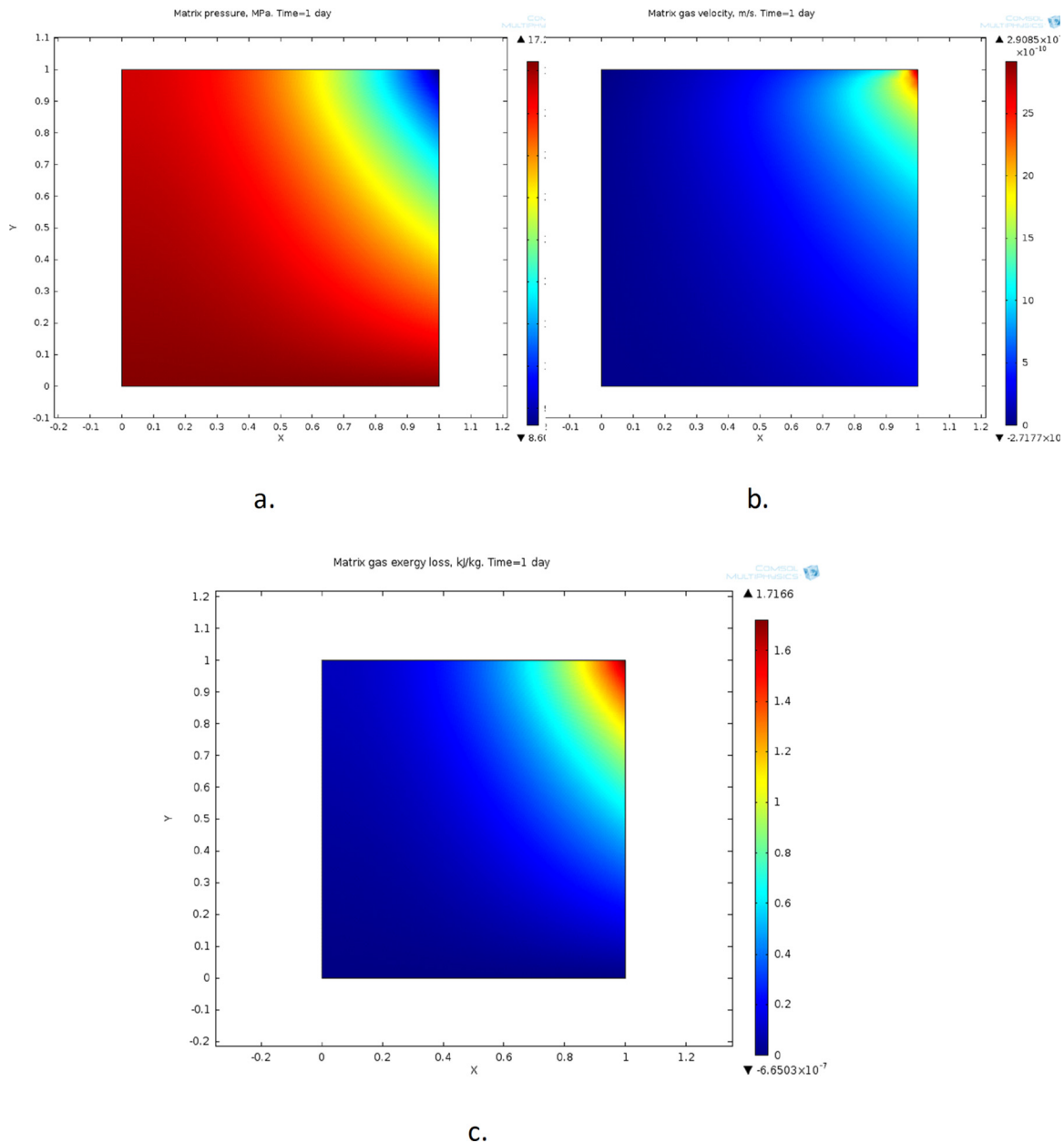


Fig. 6 Distributions in the matrix after 1 day of: (a) gas pressure (the scale is in MPa), (b) gas velocity (the scale is in 10^{-10} m/s), and (c) exergy loss (the scale is in kJ/kg)

Since the enthalpy and gravity components in this model do not change, but accounts for about 95% of the whole exergy, and the kinetic energy component is negligible, we only compared the relative change of exergy due the entropy component, ignoring the other (but large yet constant) exergy components.

To study the sensitivity of the results to the matrix parameters r , ϕ_m , P_i , L_m , and L_f , we changed them by $\pm 10\%$ and repeated the computations at these conditions. Examination of the change of gas pressure, exergy, and exergy loss relative to the original state at the matrix central point ($X=0.5, Y=0.5$) and at the point ($X=0.8, Y=0.8$) that is closer to the fracture and the well, at the nearly steady-state 15th day, has shown that in general, a $\pm 10\%$ change of the input parameters causes a change within $\pm 1\%$, except for the exergy loss change of $+8\%$ to -10% corresponding to the $\pm 10\%$ change of the initial pressure.

Specifically, it can be seen that when r increases, pressure and exergy decrease, and exergy loss increases. This is because the

increase of matrix pore-throat radius increases the pressure drop rate. The exergy loss is more sensitive to the r change than the other two. In addition, the three terms change more for a reduced pore-throat radius.

When ϕ_m increases, the pressure and exergy increase and exergy loss decreases because the increase of ϕ_m increases the gas transport and content in the matrix. Exergy loss is more sensitive to ϕ_m change than to the other two. The three terms are more sensitive to the increase of ϕ_m .

The exergy and exergy loss at point ($X=0.8, Y=0.8$) was found to be less sensitive to the parameters' variation than at the center of the matrix ($X=0.5, Y=0.5$) because the former point is also influenced by the conditions in the hydraulic fracture.

In general, a matrix with larger pore-throat radius, lower porosity, higher initial pressure, longer fractures, and smaller matrix width leads to a higher matrix exergy loss, and a matrix with

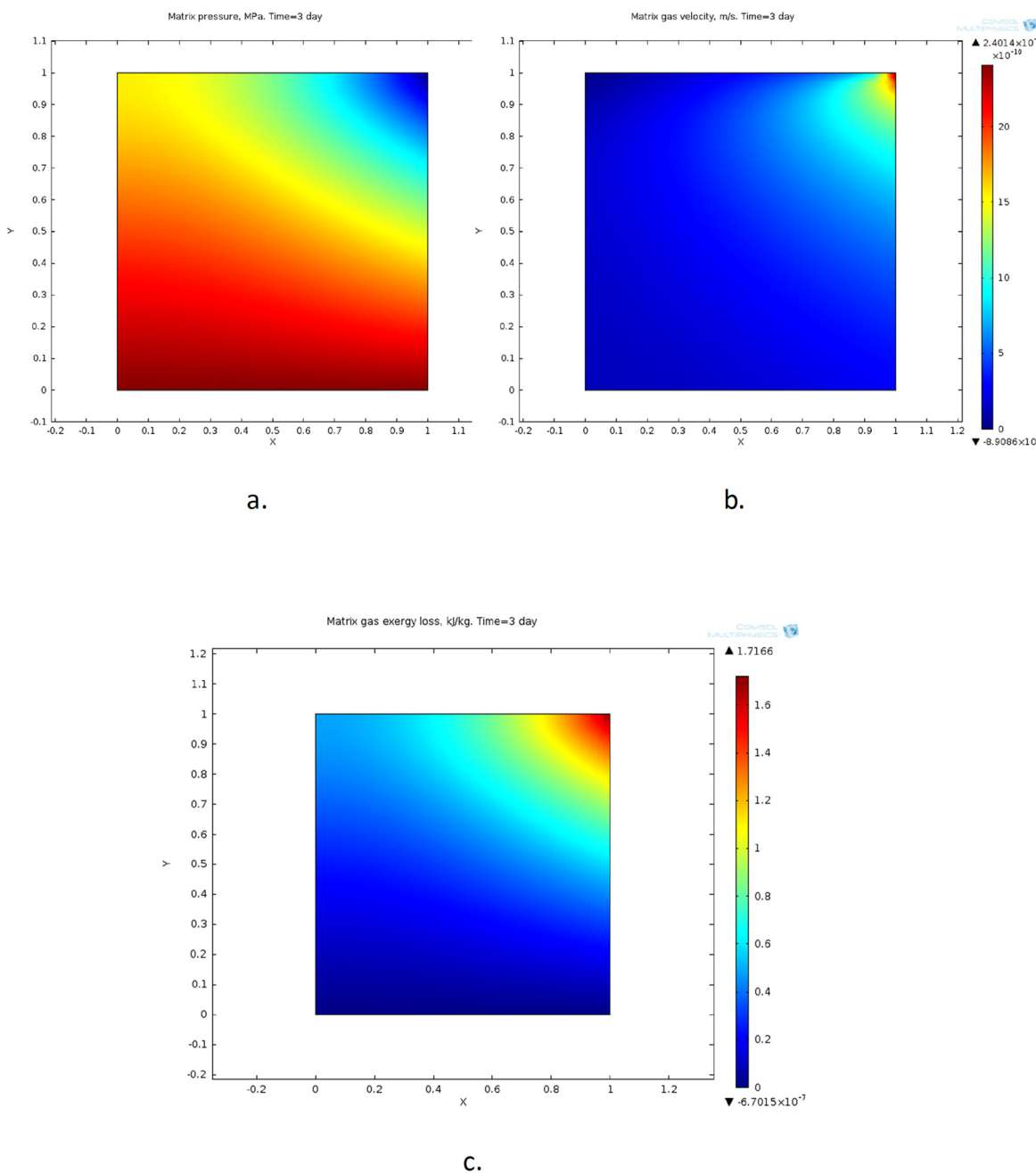


Fig. 7 Distributions in the matrix after 3 days of: (a) gas pressure (the scale is in MPa), (b) gas velocity (the scale is in 10^{-10} m/s), and (c) exergy loss (the scale is in kJ/kg)

a smaller pore-throat radius, higher porosity, lower initial pressure, shorter fracture length, and wider matrix leads to a lower exergy loss.

To study the sensitivity of the results to the fracture parameters k_f , ϕ_f , and L_f , their magnitudes were varied by $\pm 10\%$ and the change of the gas pressure, exergy, and exergy loss in the fracture relative to the origin state was computed at the middle of the fracture length, $Y=0.5$, at the 15th day by when the process became nearly stable. The results show that these changes have a negligible effect, because the gas flow velocity in a fracture is 10^5 -fold higher than the gas velocity in the matrix, causing the fracture to have a much bigger capacity for gas transport than the matrix. If the fracture porosity or permeability was reduced to the level of those in the matrix, the parameters' change will naturally have stronger influences.

2.8 Error Analysis of the Numerical Simulation. The error analysis includes assessment of errors caused by the idealization and assumptions, computational grid influence, comparison with the calculations performed by using the COMSOL, as well as comparison with some available analyses in the literature, and qualitative comparison with available experimental data.

2.8.1 Errors Caused by the Idealization and Assumptions Made for the Model. As described in Sec. 2.4.2, we adapted and used a dual-porosity model for modeling gas transport in shale reservoirs. The model has several idealizations and assumptions that may cause some errors, and the major ones and their explanations and justifications are as follows:

- (1) Water backflow was not considered, just as in the other analyses found in the literature. After hydrofracturing is

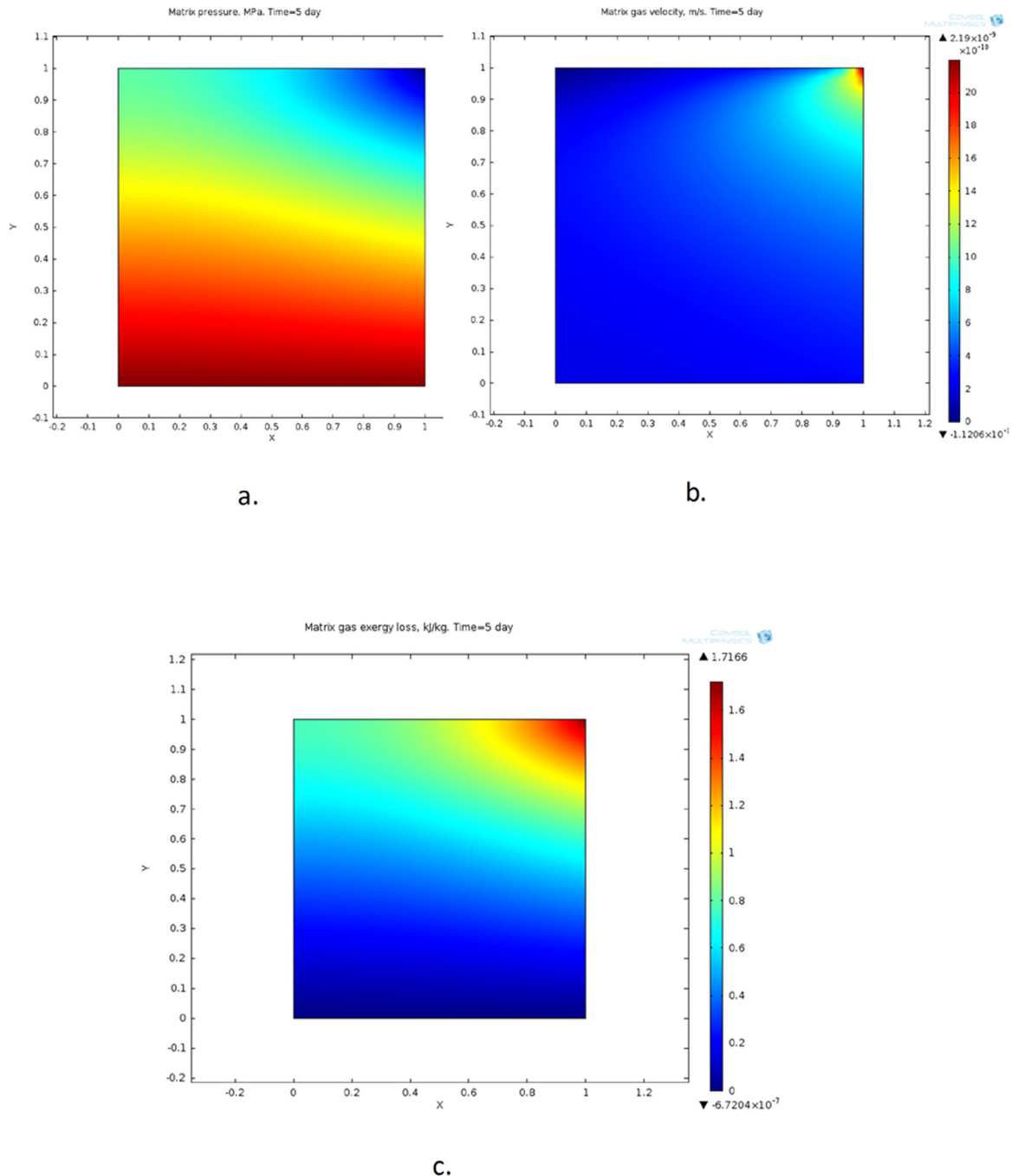


Fig. 8 Distributions in the matrix after 5 days of: (a) gas pressure (the scale is in MPa), (b) gas velocity (the scale is in 10^{-10} m/s), and (c) exergy loss (the scale is in kJ/kg)

complete and the well starts to produce gas, 10–50% of the fracturing water flows back with the produced gas, but only during the first several days. During that relatively short period, our model would overpredict the gas production rate and pressure drop, because the produced gas would have to overcome the water backflow in that period.

- (2) The boundary of the considered matrix (stimulated matrix) was in our model assumed to have a constant pressure equal to the initial reservoir pressure. In fact, the pressure of the surrounding reservoir is likely to drop over time, leading to gas production rates lower than predicted by the model. Some justifications for this assumption are that the pressure reduction takes place over a long time, typically years, and that comparison of the model predictions with actual gas play performance data during a steady production period (5–10 yrs, discussed further in Sec. 2.3.5.3) shows a good agreement.

2.8.2 Comparison to Available Simulation Results. Specific comparison was made with the well-cited paper [43], which employs a model that similarly considers Knudsen diffusion, slip flow, and apparent permeability, using the method introduced in Ref. [3], and solves the problem numerically. It presents the input

data and the output pressure distribution, which we thus were able to use in our model for testing its validity.

Most other modeling papers only focus on production estimation but did not report information about the fluid mechanics. Some relative advancements in our model are: (1) while in Ref. [40] the system was assumed to be one-dimensional radial, composed of a cylindrical tube with a horizontal well in the middle and a matrix containing fractures surrounding it, our model represents the fluid mechanics in a somewhat more realistic way, as it consists of a rectangular shale matrix and rectangular blocks with hydraulic fractures beside it, with 2D flow in the uniform matrix and one-dimensional flow in the fractures, and (2) we developed a partial differential equation (PDE) system for the model and solved it numerically to get the result, while in Ref. [43], it seems that the governing equations were solved partially by use of a correlations algorithm.

For the computation comparison, the input data from Ref. [43] were thus used with the width of the hydraulic fracture in our analysis assumed to be twice the width of their horizontal well, with all other parameters kept the same. The comparison criterion was the pressure distribution along a 100 m fracture after 1 yr, and our results were lower than those in Ref. [43] by only about 0.5–3.4%, showing a rather satisfactory agreement.

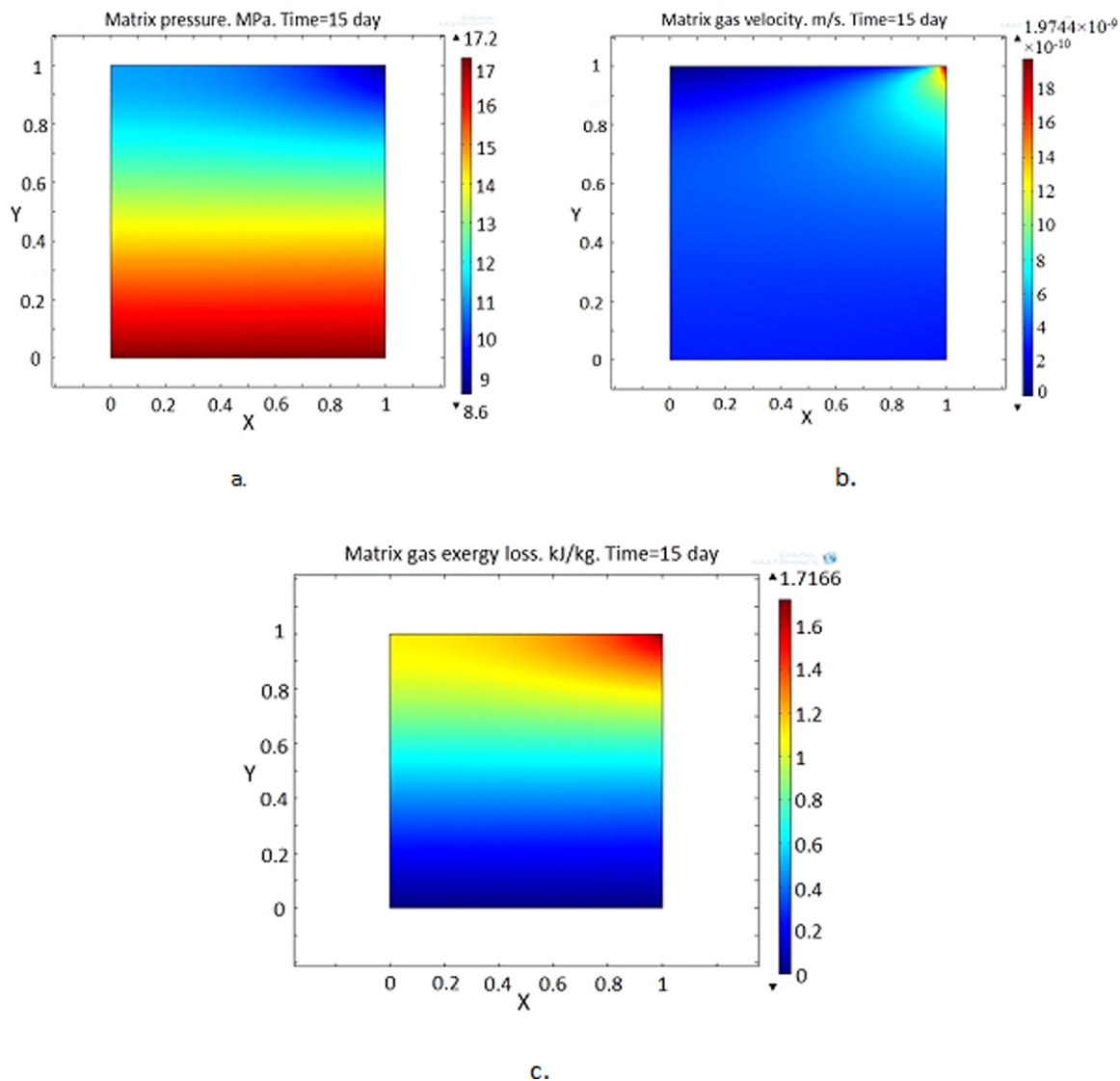


Fig. 9 Distributions in the matrix after 15 days of: (a) gas pressure (the scale is in MPa), (b) gas velocity (the scale is in 10^{-10} m/s), and (c) exergy loss (the scale is in kJ/kg)

2.8.3 Comparison With Shale Gas Plays Data. Publicly available hydrofractured shale gas play information is the production rates, and not all details are included in their simulation models. Furthermore, well production depends on the way it was made and on time (cf. Ref. [50]). We could therefore only compare the production rates predicted by our model to the range of production rates reported from different operating hydrofractured shale gas wells.

According to Refs. [51–55], the stable daily production rate is around 1.5×10^4 to 4.5×10^4 m³/day (500–1500 Mcf/day). The stable daily production rate from our model is calculated by

$$q = v \times w \times h_f \times 2 \times n_{\text{stage}} \times (P_w/P_0) \times (T_0/T) \times 3600 \times 24 \quad (30)$$

where the variables used in our model and closest to typical shale gas wells are q , the daily production rate; v , the calculated gas velocity at the exit of the hydraulic fractures = 8.5×10^{-4} m/s; w , the assumed fracture width = 0.3 m; h_f , the assumed fracture height = 1 m; the number 2 accounts for the second part of this symmetric fracture; n_{stage} is the number of fracturing stages (15 in our model); P_w , the pressure at the exit point of the hydraulic fracture = 8.6 MPa; P_0 , the pressure used to measure the flow rate (assumed here to be the dead state pressure) = 101,325 Pa; T , the temperature at the exit point of the hydraulic fracture = 423 K;

and T_0 , the temperature at which the flow rate is measured (assumed here to be the dead state temperature) = 298 K.

Using this equation, the stable production rate from our model is calculated to be $v = 3.95 \times 10^4$ m³/day, which falls well in the typical shale gas plays range of 1.5×10^4 to 4.5×10^4 m³/day. While many assumptions are made in the model, it is somewhat reassuring that the flow rates are within a realistic range for such wells.

To gain confidence in our COMSOL solution, its grid dependence was first examined by comparing the solutions for the pressure at a point in the middle of the matrix (to analyze the mesh influence on matrix gas pressure), at a point in the middle of the border of matrix and fractures (to analyze the mesh influence on matrix gas pressure at the boundary), and at a point in the middle of the fracture to see the mesh influence on the fracture gas pressure. This was done at the tenth second and at the 10⁵th second after the start. Triangular cell shapes were used, which is the COMSOL default. COMSOL offers nine levels of mesh intensity: extremely coarse, extra coarse, coarser, coarse, normal, fine, finer, extra fine, and extremely fine. Comparing our results to those obtained from using much finer grids (the COMSOL “extremely fine” mesh for the tenth second case and the “extra fine” one for the 10⁵th second case), the errors were below 0.1% for all cases except at the boundary of the tenth second case where they were below 1%. The conclusion is that the grid-related errors are negligible.

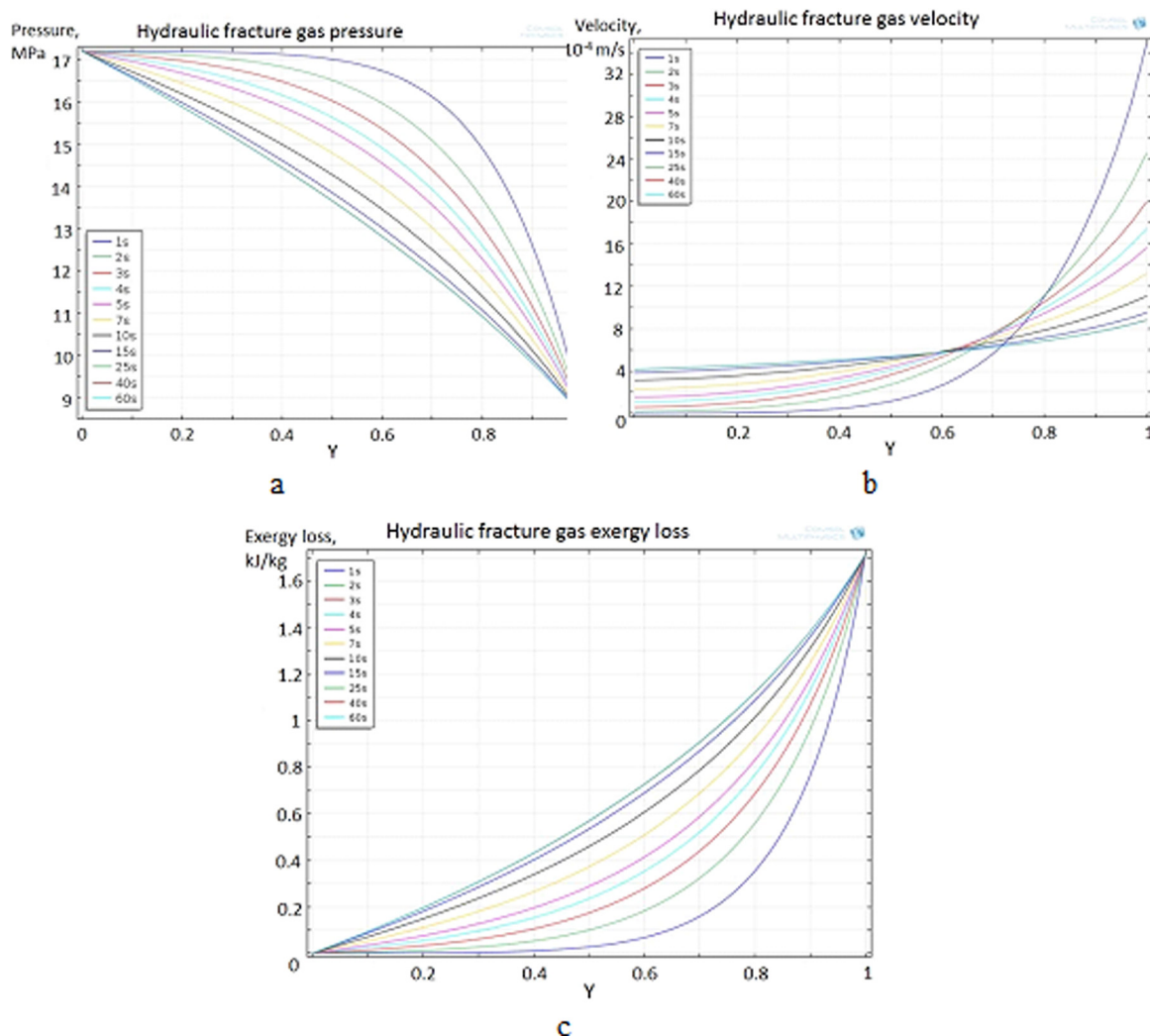


Fig. 10 Distributions in the hydraulic fracture of: (a) gas pressure (the scale is in MPa), (b) gas velocity (the scale is in m/s), and (c) exergy loss (the scale is in kJ/kg)

Finally, it is examined whether the governing Eq. (12) is satisfied at a random point and time ($X=0.8$, $Y=0.8$, 15 days) and was found that the difference between the two sides of Eq. (12) in its transient or steady-state form is no more 5.4×10^{-7} Pa/s, thus practically zero, verifying the correctness of the numerical analysis.

The error analysis steps described in the section assure acceptable confidence in the results within the given parameters.

3 Conclusions

An exergy system analysis of construction of a typical U.S. shale gas well, which includes the processes and materials exergies (embodied exergy) for drilling, casing and cementing, and hydrofracturing, was conducted. It was followed by a gas flow and intrinsic exergy numerical simulation and analysis in a gas-containing hydrofractured shale reservoir with its formed fractures, resulting in the time- and 2D space-dependent pressure, velocity, and exergy loss fields in the matrix and fractures.

Some of the key results of the system analysis show that:

- The total exergy consumption for constructing the hydrofractured shale gas well is 35.8 TJ.
- 49% of that is used for all the drilling needed for the well and casing holes.
- Hydro fracturing requires 48% of the total exergy consumption.
- The embodied exergy of all construction materials is about 9.8% of the total exergy consumption.
- The ExROI for the typical range of shale gas wells in the U.S. was found to be 7.3–87.8.
- Since the energy embodied in manufactured materials like steel and concrete is larger than the embodied exergy, the total energy consumption for constructing the hydrofractured shale gas well is 38.7 TJ, 8% higher than the exergy, with an EROI of 6.7–81. Both this EROI and the ExROI indicate a typically satisfactory return for most of the real wells considered in this example.
- Error analysis of the numerical simulation method and its results assure acceptable confidence in the results within the given parameters.
- The very slow (order of 10^{-9} m/s) gas flow velocity through the matrix points to the desirability of fracking methods that increase the matrix-fractures interfacial area. This can be accomplished by increasing the number of fractures, their lengths, and of the number of their directions, and by a smaller matrix width to thus reduce the gas flow path, all as long as excessive merging of fractures does not result in lower coverage of the drainage area; such improvements have a very small exergy penalty.
- It appears that the assumed fracture width and length are adequate to drain the flow from the pores of the matrix in this model; in other words, the flow resistance in the fracture was smaller than that in the matrix pores. This should be an important criterion in designing hydrofracturing systems.

Acknowledgment

The author is grateful to his former graduate student Yang Hu, who very significantly contributed to this study.

Nomenclature

e	= specific exergy, kJ/kg
E_{cement}	= total embodied exergy of the used cement, GJ
e_{CH_4}	= specific embodied molar exergy of methane, kJ/mol
$E_{\text{c\&c}}$	= total embodied exergy consumption of casing and cementing materials, GJ
E_{drill}	= total exergy consumption for drilling, GJ
E_{frac}	= total exergy required for the overall fracking, GJ

E_{input}	= total exergy consumption of drilling, casing and cementing, and fracturing, GJ
E_{pf}	= the total required exergy for the assumed typical fracking job, GJ
E_{proppant}	= embodied exergy of used proppant, GJ
E_{steel}	= total embodied exergy of the used steel, GJ
E_{water}	= embodied exergy of the used water, GJ
EROI	= energy return on investment, dimensionless
ExROI	= exergy return on investment, dimensionless
F	= the source term representing the gas flow from the matrix, Eq. (18), 1/s
g	= gravitational acceleration, m/s ²
h	= enthalpy, kJ/kg
k_{app}	= apparent permeability
L_f	= the length of each hydraulic fracture, m
L_m	= the half-width of each shale matrix block between two adjacent hydraulic fractures, m
M	= molar weight, kg/mol
n_{stage}	= the number of fracturing stages
P	= pressure, Pa
P_f	= required pumping power for fracking, MW
q	= flow rate, m ³ /s
Q_f	= the fracking fluid flow rate, m ³ /min
r	= equivalent pore-throat radius, m
R	= universal gas constant
s	= entropy, kJ/(kg K)
t	= time
T	= temperature, K
\mathbf{u}	= velocity vector, m/s
v	= volume, m ³
\mathbf{V}	= velocity vector, m/s
V_{methane}	= volume of produced methane needed to compensate for E_{input} , m ³
w	= fracture width, m
x	= direction parallel to the fracking well
X	= dimensionless direction x , $= x/L_m$
y	= direction perpendicular to the fracking well
Y	= dimensionless direction y , $= y/L_f$
z	= altitude above a reference level, m

Greek Symbols

α	= empirical coefficient in Eq. (8)
$(\Delta p)_f$	= the fracking pressure, MPa
ϵ_{pg}	= electrical power generation exergy efficiency, = 0.4
η_p	= efficiency of the fracking pump
μ	= dynamic viscosity, N s/m ²
ρ	= density, kg/m ³
ρ_{CH_4}	= density of methane, kg/m ³
τ_f	= time length for fracking pumping, min
ϕ	= porosity, dimensionless

Subscripts

CH_4	= methane
f	= final
hf	= hydraulic fracture
i	= initial
m	= matrix
w	= in the gas well
0	= dead state (for exergy calculations)

References

- [1] Hu, Y., 2013, "Exergy Analysis in Shale Gas Extraction Processes," M.S. thesis, Chemical and Biomolecular Engineering Department, University of Pennsylvania, Philadelphia, PA.
- [2] Ozkan, E., Raghavan, R. S., and Apaydin, O. G., 2010, "Modeling of Fluid Transfer From Shale Matrix to Fracture Network," *SPE Annual Technical Conference and Exhibition*, Florence, Italy, Sept. 19–22, Paper No. SPE 134830.
- [3] Javadpour, F., 2009, "Nanopores and Apparent Permeability of Gas Flow in Mudrocks (Shales and Siltstone)," *J. Can. Pet. Technol.*, 48(8), pp. 16–21.

- [4] U.S. Energy Information Administration, 2013, "Technically Recoverable Shale Oil and Shale Gas Resources: An Assessment of 137 Shale Formations in 41 Countries Outside the United States," U.S. Department of Energy, Washington, DC, accessed Oct. 25, 2015, <http://www.eia.gov/analysis/studies/worldshalegas/pdf/fullreport.pdf>
- [5] U.S. Energy Information Administration, 2012, "U.S. Crude Oil and Natural Gas Proved Reserves," U.S. Department of Energy, Washington, DC, <http://www.eia.gov/naturalgas/crudeoilreserves/index.cfm>
- [6] EPA, "Hydraulic Fracturing Water Cycle," U.S. Environmental Protection Agency, Washington, DC, accessed Feb. 28, 2015, <http://www2.epa.gov/hfstudy/hydraulic-fracturing-water-cycle>
- [7] Hughes, J. D., 2015, "Drilling Deeper—Part 3: Shale Gas," The Post Carbon Institute, Santa Rosa, CA, p. 153, accessed Oct. 25, 2015, http://www.postcarbon.org/wp-content/uploads/2014/10/Drilling-Deeper_PART-3-Shale-Gas.pdf
- [8] Yost, A. B., Overbey, W. K., and Carden, R. S., 1987, "Drilling a 2,000-ft Horizontal Well in the Devonian Shale," 62nd SPE Annual Technical Conference and Exhibition, Dallas, TX, Sept. 27–30; available at: <http://www.netl.doe.gov/kmd/cds/disk7/disk1/EGS%5CDrilling%20a%202,000-ft%20Horizontal%20Well%20in%20the%20Devonian%20Shale.pdf>
- [9] Maurer, W., 1995, "Recent Advances in Horizontal Drilling," *J. Can. Pet. Technol.*, **34**(9), p. PETSOC-95-092.
- [10] Maidla, E., Hacı, M., and Wright, D., 2009, "Case History Summary: Horizontal Drilling Performance Improvement Due to Torque Rocking on 800 Horizontal Land Wells Drilled for Unconventional Gas Resources," *SPE Annual Technical Conference and Exhibition*, New Orleans, LA, Oct. 4–7, Paper No. SPE-123161-MS.
- [11] Harper, J. A., 2008, "The Marcellus Shale—An Old 'New' Gas Reservoir in Pennsylvania," *PA Geol.*, **38**(1), pp. 2–13.
- [12] Marcellus Center for Outreach and Research (MCOR), 2015, "Cross Section of a Typical Horizontal Marcellus Well," Pennsylvania State University, Earth-Engineering Sciences Building, University Park, PA, accessed Oct. 25, 2015, http://www.marcellus.psu.edu/images/horizontal_well.gif
- [13] Marcellus Shale Coalition, 2015, "Well Casing," Marcellus Shale Coalition, Pittsburgh, PA, accessed Oct. 25, 2015, <http://marcelluscoalition.org/marcellus-shale/production-processes/casing-the-well>
- [14] Chong, K. K., Grieser, W., Passman, A., Tamayo, H., Modeland, N., and Burke, B., 2010, "A Completions Guide Book to Shale-Play Development: A Review of Successful Approaches Toward Shale-Play Stimulation in the Last Two Decades," Canadian Unconventional Resources and International Petroleum Conference, Calgary, Canada, Oct. 19–21.
- [15] Agrawal, A., Wei, Y., Cheng, K., and Holditch, S., 2010, "A Technical and Economic Study of Completion Techniques in Five Emerging U.S. Gas Shales," *SPE Annual Technical Conference and Exhibition*, Florence, Italy, Sept. 20–22, Paper No. SPE-135396-MS.
- [16] Lior, N., 2002, "Thoughts About Future Power Generation Systems and the Role of Exergy Analysis in Their Development," *Energy Convers. Manag. J.*, **43**(9–12), pp. 1187–1198.
- [17] Lior, N., Sarmiento-Darkin, W., and Al-Sharqawi, H. S., 2006, "The Exergy Fields in Transport Processes: Their Calculation and Use," *Energy*, **31**(5), pp. 553–578.
- [18] Shale Reporter, "How Deep in the Ground is the Shale Layer?," Calkins Media, Levittown, PA, accessed Feb. 28, 2015, http://www.shalereporter.com/resources/faq/geology/article_2f36d46a-340c-11e2-9928-001a4bcf6878.html
- [19] PetroWiki, 2015, "Horizontal Wells," Society of Petroleum Engineers, Richardson, TX, accessed Oct. 25, 2015, http://petrowiki.org/Horizontal_wells
- [20] Polsky, Y., Capuano, L., Finger, J., Huh, M., Knudsen, S., Mansure, A., Raymond, D., and Swanson, R., 2008, "Enhanced Geothermal Systems (EGS) Well Construction Technology Evaluation Report," Sandia National Laboratories, Albuquerque, NM, Report No. SAND2008-7866, accessed Oct. 25, 2015, http://www1.eere.energy.gov/geothermal/pdfs/egs_well_construction.pdf
- [21] Hermann, W. A., 2006, "Quantifying Global Exergy Resources," *Energy*, **31**(12), pp. 1685–1702.
- [22] Rudzinski, W. E., Aminabhavi, T. M., Sassman, S., and Watkins, L. M., 2000, "Isolation and Characterization of the Saturate and Aromatic Fractions of a Maya Crude Oil," *Energy Fuels*, **14**(4), pp. 839–844.
- [23] Office of Fossil Energy and National Energy Technology Laboratory, 2009, "Modern Shale Gas Development in the United States: A Primer," U.S. Department of Energy, Washington, DC, accessed Oct. 25, 2015, <http://energy.gov/fe/downloads/modern-shale-gas-development-united-states-primer>
- [24] API, 2011, "Specification ISO 11960:2011 Petroleum and Natural Gas Industries—Steel Pipes for Use as Casing or Tubing for Wells," 5CT, 9th ed., *Specification for Casing and Tubing*, American Petroleum Institute, Washington, DC, accessed Oct. 25, 2015, <http://www.api.org/certification-programs/api-monogram-program-and-apigr/purchasing-guidelines-handbook-updates>
- [25] Szargut, J., 2005, *Exergy Method: Technical and Ecological Applications*, WIT Press, Ashurst, UK.
- [26] Koroneos, C., Roumbas, G., and Moussiopoulos, N., 2005, "Exergy Analysis of Cement Production," *Int. J. Exergy*, **2**(1), pp. 55–68.
- [27] Hammond, G., and Jones, C., 2011, "Inventory of Carbon & Energy (ICE) Version 2.0," University of Bath, Bath, UK, <http://www.circularecology.com/embodied-energy-and-carbon-footprint-database.html#.Vji2Dis2aXc>
- [28] Arthur, J. D., Bohm, B., and Layne, M., 2008, "Hydraulic Fracturing Considerations for Natural Gas Wells of the Marcellus Shale," GWPC Annual Forum, Cincinnati, OH, Sept. 21–24, accessed Oct. 25, 2015, http://www.dec.ny.gov/docs/materials_minerals_pdf/GWPCMarcellus.pdf
- [29] Rees, S., 2009, "Creating Value in the Marcellus Under the New SEC Rules," Hart Developing Unconventional Gas—Making the Marcellus Pay Pittsburgh, PA, Oct. 19.
- [30] Bullin, K., and Krouskop, P., 2009, "Composition Variety Complicates Processing Plans for U.S. Shale Gas," *Oil Gas J.*, **107**(10), pp. 50–55.
- [31] Mu, S. R., and Zhang, S. C., 2012, "Numerical Simulation of Shale Gas Production," *Adv. Mat. Res.*, **402**, pp. 804–807.
- [32] Zhou, D., Zheng, P., Peng, J., and He, P., 2015, "Induced Stress and Interaction of Fractures During Hydraulic Fracturing in Shale Formation," *ASME J. Energy Resour. Technol.*, **137**(6), p. 062902.
- [33] Du, C. M., Zhang, X., Zhan, L., Gu, H., Hay, B., Tushingham, K., and Ma, Y., 2010, "Modeling Hydraulic Fracturing Induced Fracture Networks in Shale Gas Reservoirs as a Dual Porosity System," CPS/SPE International Oil & Gas Conference and Exhibition, Beijing, China, June 8–10.
- [34] Kalantari-Dahaghi, A., 2011, "Systematic Approach to Numerical Simulation and Modelling of Shale Gas Reservoirs," *Int. J. Oil, Gas Coal Technol.*, **4**(3), pp. 209–243.
- [35] Silin, D., and Kneafsey, T., 2012, "Shale Gas: Nanometer-Scale Observations and Well Modelling," *J. Can. Pet. Technol.*, **51**(6), pp. 464–475.
- [36] Freeman, C. M., Moridis, G., Ilk, D., and Blasingame, T. A., 2013, "A Numerical Study of Performance for Tight Gas and Shale Gas Reservoir Systems," *J. Pet. Sci. Eng.*, **108**, pp. 22–39.
- [37] Shabro, V., Torres-Verdin, C., and Sepehrnoori, K., 2012, "Forecasting Gas Production in Organic Shale With the Combined Numerical Simulation of Gas Diffusion in Kerogen, Langmuir Desorption From Kerogen Surfaces, and Advection in Nanopores," *SPE Annual Technical Conference and Exhibition*, San Antonio, TX, Oct. 8–10, Paper No. SPE-159250-MS.
- [38] Brohi, I., Pooladi-Darvish, M., and Aguilera, R., 2011, "Modeling Fractured Horizontal Wells as Dual Porosity Composite Reservoirs—Application to Tight Gas, Shale Gas and Tight Oil Cases," *SPE Western North American Regional Meeting*, Anchorage, AK, May 7–11, Paper No. SPE-144057-MS.
- [39] Du, C. M., Zhan, L., Li, J., Zhang, X., Church, S., Tushingham, K., and Hay, B., 2011, "Generalization of Dual-Porosity-System Representation and Reservoir Simulation of Hydraulic Fracturing-Stimulated Shale Gas Reservoirs," *SPE Annual Technical Conference and Exhibition*, Denver, CO, Oct. 30–Nov 2, Paper No. SPE-146534-MS.
- [40] Abdul, H. J., Samandarli, O., and Wattenbarger, B. A., 2011, "New Type Curves for Shale Gas Wells With Dual Porosity Model," *Canadian Unconventional Resources Conference* Alberta, Canada, Nov. 15–17, Paper No. SPE-149367-MS.
- [41] Azom, P., and Javadpour, F., 2012, "Dual-Continuum Modeling of Shale and Tight Gas Reservoirs," *SPE Annual Technical Conference and Exhibition*, San Antonio, TX, Oct. 8–10, Paper No. SPE-159584-MS.
- [42] Dehghanpour, H., and Shirdel, M., 2011, "A Triple Porosity Model for Shale Gas Reservoirs," *Canadian Unconventional Resources Conference*, Alberta, Canada, Nov. 15–17, Paper No. SPE-149501-MS.
- [43] Shabro, V., Torres-Verdin, C., and Javadpour, F., 2011, "Numerical Simulation of Shale Gas Production: From Pore-Scale Modeling of Slip-Flow, Knudsen Diffusion, and Langmuir Desorption to Reservoir Modeling of Compressible Fluid," *North American Unconventional Gas Conference and Exhibition*, Woodlands, TX, June 14–16, Paper No. SPE-144355-MS.
- [44] Li, J., Guo, B., and Feng, Y., 2013, "An Analytical Solution of Fracture-Induced Stress and Its Application in Shale Gas Exploitation," *ASME J. Energy Resour. Technol.*, **136**(2), p. 023102.
- [45] Dokhani, V., Yu, M., Miska, S. Z., and Bloys, J., 2015, "The Effects of Anisotropic Transport Coefficients on Pore Pressure in Shale Formations," *ASME J. Energy Resour. Technol.*, **137**(3), p. 032905.
- [46] Osholake, T., Wang, J. Y., and Ertekin, T., 2012, "Factors Affecting Hydraulically Fractured Well Performance in the Marcellus Shale Gas Reservoirs," *ASME J. Energy Resour. Technol.*, **135**(1), p. 013402.
- [47] Dunbar, W. R., Lior, N., and Gaggioli, R. A., 1992, "The Component Equations of Energy and Exergy," *ASME J. Energy Resour.*, **114**(1), pp. 75–83.
- [48] Wischniewski, B., 2015, "Calculation of Thermodynamic State Variables of Methane," Peace Software, Berlin, accessed Oct. 25, 2015, http://www.peace-software.de/einige_werte/methan_e.html
- [49] COMSOL, 2015, "Multiphysics® Software," COMSOL Inc., Burlington, MA, accessed Oct. 25, 2015, <http://www.comsol.com/products>
- [50] King, G. E., 2010, "Thirty Years of Gas Shale Fracturing: What Have We Learned?," *SPE Annual Technical Conference and Exhibition*, Florence, Italy, Sept. 19–22, Paper No. SPE-133456-MS.
- [51] Vartit, V., 2012, "Alternative Interpretations of Shale Gas/Oil Rate Behavior Using a Triple Porosity Model," *SPE Annual Technical Conference and Exhibition*, San Antonio, TX, Oct. 8–10, Paper No. SPE 159703.
- [52] Samandarli, O., Al Ahmadi, H. A., and Wattenbarger, R. A., 2011, "A New Method for History Matching and Forecasting Shale Gas Reservoir Production Performance With a Dual Porosity Model," *North American Unconventional Gas Conference and Exhibition*, Woodlands, TX, June 14–16, Paper No. SPE-144335-MS.
- [53] Walton, I. C., and Erkal, A., 2009, "Evaluation of Shale Gas Productivity Using a New Asymptotic Model. SPE Production and Operations Symposium," Oklahoma City, OK, Apr. 4–9, pp. 420–434.
- [54] Esmaili, S., Kalantari Dahaghi, A., and Mohaghegh, S. D., 2012, "Modeling and History Matching of Hydrocarbon Production From Marcellus Shale Using Data Mining and Pattern Recognition Technologies," *SPE Eastern Regional Meeting*, Lexington, KY, Oct. 3–5, Paper No. SPE-161184-MS.
- [55] Cipolla, C. L., Lolon, E. P., Erdle, J. C., and Tathed, V., 2009, "Modeling Well Performance in Shale-Gas Reservoirs," *SPE/EAGE Reservoir Characterization & Simulation Conference*, Abu Dhabi, UAE, Oct. 19–21, Paper No. SPE-125532-MS.